A z-axis tunneling microscope for undergraduate labs

Randy Lindgren, Wesley Kozan, Noah Fuerst, Douglas Knapp, and Joshua P. Veazey*
Department of Physics, Grand Valley State University, Allendale, MI 49401

(Dated: July 6, 2022)

Abstract

We present the design and construction of a laboratory apparatus that provides advanced undergraduates with hands-on observations of electron quantum tunneling and the electronic density of states of various materials. The instrument is inspired by the scanning tunneling microscope (STM), but its implementation is simplified by limiting the tip motion to the single dimension along the tip-sample separation (z-axis); we refer to the device as the z-axis tunneling microscope (ZTM). Students are able to use the ZTM to measure electron tunneling probability as a function of barrier width, estimate relative material work functions, and observe differences in local electronic structure between metals, semimetals, and semiconductors. We share results obtained by third-year undergraduate physics students using the instrument for their final projects in an advanced instructional lab course.

I. INTRODUCTION

First- and second-year undergraduate students often arrive with enthusiasm for learning about the surprising effects of quantum mechanics, including quantum tunneling. In coursework, however, their initial interest may get bogged down by abstract representations of the tunnel barrier. Studies of material properties like electronic structure can also challenge students because they are abstract and without many experimental opportunities. Pictorial representations of tunneling experiments, such as the scanning tunneling microscope (STM), can relieve some abstraction. Many published examples of homebuilt and student-built STMs have been valuable for expanding access.[1–4] However, developing a corresponding hands-on STM lab adds complexity, and analysis of images may distract from the core learning objectives identified above.

We propose the following simpler solution for undergraduate instructional labs: a tunneling microscope that only moves the tip along the single axis defined by the tip-sample separation, an instrument we dub the *z-axis tunneling microscope* (ZTM). A schematic and photo of the key components of the ZTM are shown in Fig. 1. Unlike the STM, the ZTM's tip does not scan laterally; like the STM, the ZTM operates in ambient conditions at room temperature. As indicated in Fig. 1 by the voltages V_{piezo} and Preamp Output, we designed the instrument with the presumption that it would interface with electronics and data acquisition equipment already existing in undergraduate programs.

Two main goals for the experiments facilitated by the ZTM are the observation of the tunneling current's exponential dependence on the tip-sample separation gap (I-z), and the observation of differences in electronic structure between various materials via tunneling spectroscopy. As we will show in the following sections, the instrument accomplishes these goals, and it can distinguish differences in electronic density of states for different classes of conducting solids, e.g., metals, semimetals, and semiconductors. Additionally, we have used the instrument in a point contact spectroscopy mode.[5] At our four-year, primarily undergraduate institution, third-year physics majors in an advanced instructional lab course have worked with the fully assembled apparatus (pictured in Fig. 2), and some of their data are presented here. Given its simplicity, the ZTM can be used in instructional labs at other levels, beginning with the sophomore modern physics course.

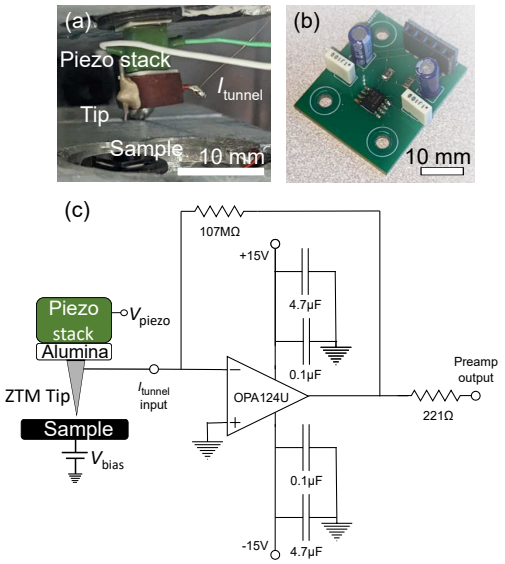

FIG. 1. (a) Photograph of the ZTM's tip-sample configuration. The sample is mounted on a stainless steel disk, held in place by a nickel-coated magnet. A piezo stack controls the tip-sample separation and is electrically isolated by a thin piece of alumina. (b) Photograph of the preamp circuit on custom printed circuit board. (c) Circuit diagram of the preamp with schematic of tip-sample configuration. The circuit is a current amplifier with 107-MΩ feedback resistor for a gain of $\sim 10^8$ V/A. A pair of large and small decoupling capacitors are connected in parallel with the power supply lines to prevent feedback oscillations. To produce a net tunneling current between the tip and sample, a bias is applied to the sample relative to the tip.

II. THEORETICAL BACKGROUND

Vacuum quantum tunneling into a metallic tip was first reported by Binnig *et al.* in 1982.[6] With the tip's lateral position fixed, the current was recorded as a function of the tip's vertical distance from the sample (I-z). This (vacuum- or air-filled) sample-tip gap, which is present in both a STM and ZTM, serves as the tunneling barrier for an electron and is most simply modeled as a one-dimensional trapezoidal barrier of average height U [Fig. 3(a)]. Undergraduates theoretically analyze this model during either their sophomore-level (modern physics) or upper-level quantum mechanics lecture courses and find that the

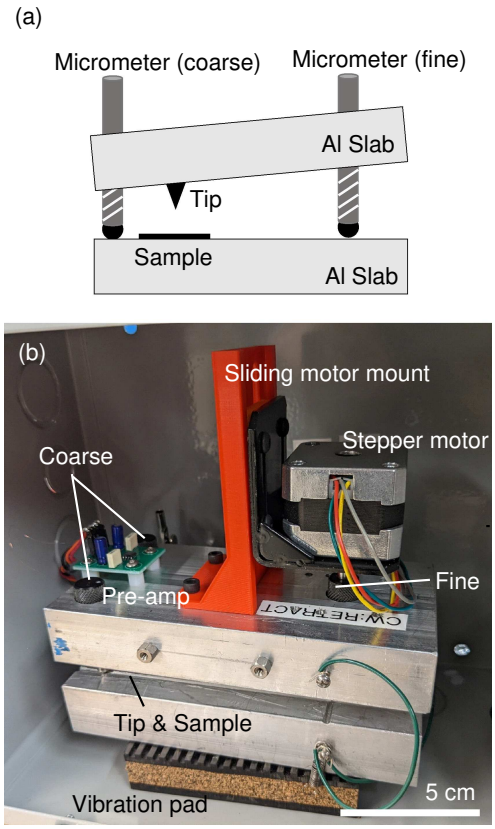

FIG. 2. (a) Schematic of the body of our instrument. Two coarse and one fine adjust micrometer screws bring the tip within 1 mm of the sample before engaging the piezo approach algorithm. The tip and sample are mounted near the coarse approach screws to give a mechanical advantage to the fine adjust. (b) Photograph of the body of our instrument. The pre-amp is mounted close to the tip. A stepper motor is mounted on a sliding bracket that was custom-fit and 3D-printed. The stepper motor controls the fine approach knob. The vibration pad isolates building vibrations.

solution to the time-independent Schrödinger equation predicts a tunneling probability that is exponential with barrier width Δz,

$$|\psi(x)|^2 \propto e^{-2\sqrt{\frac{2m(U-E)}{\hbar}}\Delta z} \approx e^{-A\sqrt{\Phi}\Delta z}$$

where m is the mass of an electron, Φ is the work function of the material, and $A = 2\sqrt{\frac{2m}{\hbar}} \approx 1.025\ \mathrm{eV}^{-1/2}\text{Å}^{-1}$. In this approximation, we take the energy E of the electron to be much less than the barrier height U. Thus, $(U - E) \approx \Phi$. When plotted on semilog axes, the slope of the I-z graph is then $-1.025\ \mathrm{eV}^{-1/2}\text{Å}^{-1}\sqrt{\Phi}$. The accuracy of the work function is higher when both tip and sample are dry, as in ultra-high vacuum. However, a STM generally does not require vacuum conditions for achieving atomic resolution for some materials in air, including the atomic structure of highly-oriented pyrolytic graphite (HOPG)[7] and the room-temperature charge-density wave (CDW) material, $CeTe_3$.[8]

Likewise, measurement of the local electronic density of states as a function of bias voltage is also accessible in ambient conditions. When using the square tunneling barrier approximation as we have done above, the Bardeen model for tunneling[9] predicts the tunneling current to be

$$I = \frac{4\pi e}{\hbar} \int_0^{eV} \rho_{tip}(E - eV)\rho_{sample}(E)T(E, V, d)\, dE,$$

where ρ_{tip} and ρ_{sample} are the electronic densities of states of the tip and sample, respectively, and $T(E, V, d)$ is the transmission probability at energy E, bias V, and barrier width d.[10] Assuming constant metallic tip density of states and small bias voltages, the derivative of the current with respect to voltage may be approximated as

$$\frac{dI}{dV} \propto \rho_{sample}(eV).$$

Thus, the differential conductance $\mathrm{d}I/\mathrm{d}V$ of the tunnel junction between the tip and sample is proportional to the local electronic density of states, and many electronic features can be inferred from an I-V curve alone.[11] Tunneling I-V curves also have high enough thermal resolution at room temperature to measure other electronic features like the charge density wave (CDW) gap in $CeTe_3$.[8] The approximation also assumes zero temperature. However, the thermal resolution at room temperature ($3.5\ k_BT \sim 90$ meV) is sufficient to distinguish the electronic density of states belonging to semiconductors from those of metals and semimetals.

III. INSTRUMENT DESIGN AND CONSTRUCTION

Tunneling currents are small (pA-nA). The current-voltage preamp circuit [Fig. 1(c)] we built has a low-noise op-amp (OPA124U) and is modeled after Dan Berard's STM preamp

circuit.[4] With the 107-MΩ feedback resistor, our circuit has a gain of $\sim 10^8$ V/A. Decoupling capacitors are attached in parallel to the op-amp power supply lines to minimize feedback oscillations. The circuit is integrated into a custom printed circuit board (see supplementary material for the custom Eagle .brd file) and mounted on the aluminum body near the tip.

The body of the ZTM is constructed from two aluminum slabs (1×3×6 in) —one with the tip attached and the other with the sample attached. Figure 2 shows a photograph and schematic of the ZTM body. Two coarse-approach micrometer screws (1/4–80), which are mounted right next to the tip and sample, bring the tip to within 1 mm of the surface. To reduce the tip-sample approach rate the fine adjustment micrometer screw (1/4–80) is mounted at the far end of the aluminum body, giving a mechanical advantage of approximately 60:1. The advancement of the micrometer screw combined with the levered mechanical advantage means the tip approaches the surface at a rate of approximately 5 μm/revolution of the fine screw. A stepper motor (NEMA-17) is attached to the fine-adjustment screw, in order to automate the approach. To attach the stepper motor, we drilled a hole in the top of the micrometer knob to fit the motor shaft. We then added a set screw through the side of the knob to hold the shaft firmly in place. An optional control board (SparkFun ROB 12779) interfaced the motor with our DAQ card.

The following standard tip-approach algorithm is used: after each step, a piezo actuator attached to the tip is extended to search for the surface. If the surface is not found, the piezo fully retracts the tip, and the stepper motor advances the fine micrometer knob another step. The process repeats until the software detects a current greater than the user-defined set point. The piezo then retracts the tip for safety and hands control over to the user. Because there is no topographic imaging (only I-z and I-V curves), the feedback loop required for imaging in STM is not necessary here (the feedback is typically shut off when using STM for I-z or I-V). However, monitoring the current by the user while the tip is in range could help prevent a tip crash from thermal drift (expansion and contraction of the piezo). Optional incorporation of a feedback loop may help prevent this from happening, but it should be turned off for I-z and I-V acquisition. These issues are discussed further in Sec. V.

The NEMA-17 stepper motor has 200 steps per revolution but can be operated in one-eighth steps, resulting in an approach as small as 3 nm per eighth-step. To avoid a tip crash, the full range of the piezo extension need only be larger than the approach per step of the stepper motor. For our piezo stack (Thorlabs PC4FL), a 10-Volt range is sufficient to

extend the piezo at least 250 nm. Likewise, the piezo extension is approximately 0.2 Å/mV, allowing sufficient z-resolution for the I-z data acquisition. The stepper motor is attached to both the top aluminum plate and the fine adjustment screw, the latter of which must move independently of the top plate. As a result, we designed and 3D-printed a sliding bracket that supports the motor while allowing it to move along with the fine-adjustment screw (Fig. 2).

The tip holder is a syringe needle (25 gauge, Sanants 30-06-2505) that is epoxied onto a phenolic standoff. Tips are mechanically cut from Pt:Ir (80:20) wire (0.2 mm diameter), as they are more inert in ambient conditions than other common tip materials like tungsten. Slightly bending the tip wire allows it to be held firmly in the syringe. The z-piezo actuator is attached to the standoff with a thin piece of alumina (Thorlabs PKFEP4) sandwiched between to electrically isolate the two. The tunneling currents are small ($\sim$ 0.1-1.0 nA), so to minimize noise from capacitive coupling, a very fine gold wire (40 AWG) is epoxied directly to the syringe, and then soldered directly to the inverting input of the op-amp on the preamp board. The sample puck is attached to the bottom piece of the aluminum body via a conducting, nickel-coated magnet (KJ Magnetics, D54). A short length of enameled magnet wire (24 gauge, Fisher S4828B) applies the bias to the sample while the tip is held at a virtual ground. For vibration isolation, the entire aluminum body sits on a rubber/cork appliance pad (PneumaticPlus, PP-CP) and is housed in a box lined with acoustic panels during data acquisition. The device has only been operated in the basement of our building, where vibrations are smallest. We have not tested it on upper floors. For electrical isolation, the box is also lined with grounded aluminum foil.

The ZTM instrument we built could interface with any homebuilt or commercial electronics controller. In our implementation, we control the ZTM and acquire data via a National Instruments USB-6259 DAQ card and LabVIEW, infrastructure previously existing for our advanced lab courses. The 10 V output limit of the DAQ card is sufficient to extend our z-piezo at least the 250 nm necessary for the approach algorithm described above, which prevents the need for an additional high-voltage piezo amplifier.

TABLE I. Components for our ZTM build, priced in US dollars.

Item	Source	Price (USD)
Aluminum slabs	eBay	40
Micrometer screws and bushings (3)	McMaster-Carr (97424A590, 98625A960)	51
NEMA-17 Motor	Adafruit (324)	14
Stepper Motor Control Board	Sparkfun (ROB12779)	16
Piezo stack	Thorlabs (PC4FL)	81
Alumina chips	Thorlabs (PKFEP4)	1
Phenolic standoff	Digikey (36-386-ND)	1
Pt:Ir tip wire	Nanoscience Instruments (20105)	124
25G syringe	Sanants 30-06-2505 (20-pack)	6
Sample holder magnet	K&J Magnetics (D54)	1
OPA 124U	Digikey	6
Anti-vibration pad	PneumaticPlus (PP-CP)	3
Acoustic panels	Foamily (12packacousticfoam1)	10
Pre-amp printed circuit board (custom)	PCBWay	3
Totals		357

TABLE II. Samples purchased, priced in US dollars.

Item	Source	Price (USD)
HOPG	Nanoscience Instruments (30102)	45
Au	Ted Pella (260374-G)	77 (for 2)
p-type Si chips (5×5 mm)	Ted Pella (16008)	110 (for 270)

IV. RESULTS

Figure 3 shows representative I-z curves acquired by the ZTM for two different materials: highly-oriented pyrolytic graphite (HOPG) and Au evaporated on glass. Each curve in Fig. 3 was acquired with a fixed sample bias of 50 mV. Students first plot an I-z curve on linear axes to observe the exponential dependence on tip-sample separation, as shown for HOPG in Fig. 3(a). Because finding the precise location of the sample surface would result in a tip

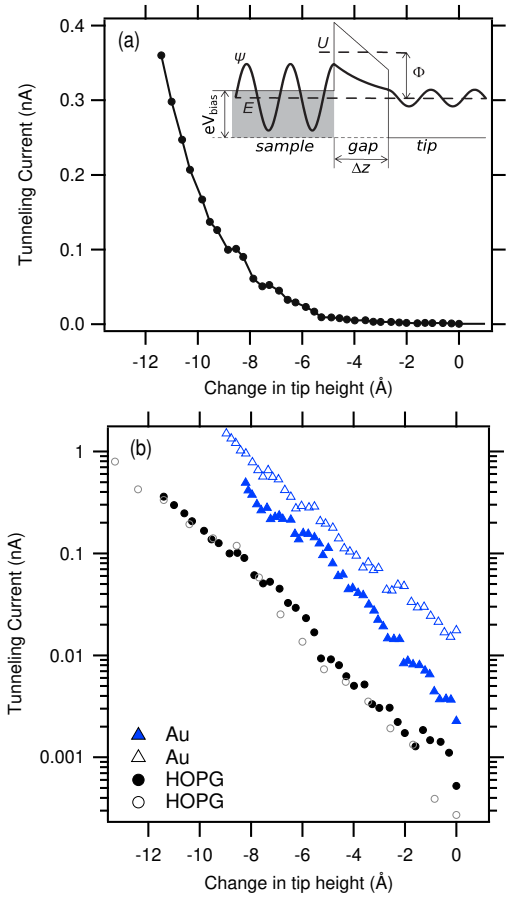

FIG. 3. Current versus tip height (relative to starting height). (a) Representative I-z curve for HOPG showing exponential dependence of the tunneling current on the tip-sample separation. Inset: 1-D model for tunneling through a potential barrier. (b) Representative I-z curves for two different materials: Au and HOPG. The data are linear when plotted on semi-log axes.

crash, current is plotted against changes in the tip's height above the sample surface, relative to its original height at the beginning of the data run, with no loss of pertinent information. From these acquired data, students are able to observe the exponential dependence of the tunneling current on the tip-sample separation (i.e., the tunneling barrier width).

As shown in Fig. 3(b), the I-z data are linear when plotted on semi-log axes, verifying the exponential relationships for both HOPG and Au. Linear fits to the semi-log plot in Fig. 3(b) yield work functions of 0.34 eV for HOPG and 0.47 eV for Au. These values are roughly an order of magnitude smaller than the known work functions for each material, which is expected when performing these experiments with the humidity levels of ambient conditions.[6] Despite being limited to ambient conditions, students still observe an exponential dependence that varies with different materials.

Tunneling spectroscopy is another way to probe differences in the electronic structure of materials with the ZTM. Figure 4 consists of data acquired by advanced physics lab students as part of their final course projects. It shows representative I-V curves comparing HOPG (a semimetal) with Au (a metal). The students observe differences in electronic structure consistent with expectations for semimetals and metals. HOPG shows an increase in the density of states at higher sample bias voltages (associated with higher energies). The I-V characteristics of Au are of nearly constant slope, consistent with expectations for metals. This comparison allows for discussion of and experimental verification of differences in electronic structure. Figures 4(a) and 4(b) display sets of three curves for HOPG and Au, respectively, showing that the data acquired by students are reproducible and low-noise. Each curve from the set was taken at the same location on its respective material. Figure 4(c) compares one representative curve from each material side by side.

The undergraduate advanced lab students analyzed the curves in a simplified, qualitative manner as described above. A more accurate model for the I-V curves would incorporate both the theoretical density of states and the enhanced transmission probability as the electron energy E approaches the barrier height U. While a quantitative analysis is beyond the scope of our first-semester advanced lab course, it may explain the weak bending at higher bias, and it is likely the reason why the Au curves are not perfectly linear. Such a possibility was discussed qualitatively with the students. Overall, this portion of the experiment facilitated instruction and engagement in independent study on electronic structure of materials for the first time in the careers of our advanced lab students.

For analysis of a semiconducting sample, the advanced lab students chose p-type Si. Students were given some background instruction on electronic band gaps in semiconductors and then predicted they would observe a band gap of about 1.1 eV. Instead, the I-V curves were highly rectifying, indicating the presence of a Schottky contact (Fig. 5). Follow-up

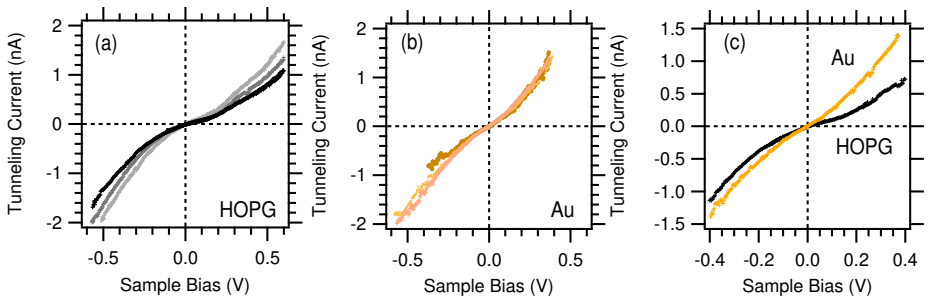

FIG. 4. Current versus voltage curves acquired by advanced lab students from different materials. (a) Three representative I-V curves acquired on HOPG. (b) Three representative I-V curves acquired on Au. (c) Comparison of one Au (metal) curve with one HOPG (semi-metal) curve showing qualitative differences in the local density of states for these materials.

discussion with students about sources of Schottky barriers explored possible causes. We note that the sample was mounted to a stainless steel disk via conductive epoxy with colloidal silver particles. However, a more likely explanation for the rectifying behavior is that the metallic Pt:Ir tip came into contact with the Si surface upon approach. The purchased p-type Si sample (Ted Pella 16008) had donor concentrations of order 10^{15}–10^{16} cm^{-3}. The tip either deposited metal on the surface or remained in a point contact configuration. Because the experiment was performed in ambient conditions, we assumed the presence of a thin, insulating SiO_2 layer that forms on the surface of Si outside of high vacuum. While the layer can be thin enough to tunnel through, its presence would have made a tip crash more probable than a pristine Si surface. The observation of the Schottky contact suggests that the ZTM could be useful for another application in advanced lab—Point Contact Spectroscopy.[5] For example, highly-doped Si has previously been used in point-contact spectroscopy studies of Schottky barriers in vacuum.[12]

V. DRIFT

As is familiar with scanning probe microscopy methods, the relative position of the tip and sample in our device may experience lateral and/or vertical drift. For example, thermal expansion and contraction of the scan head components can occur due to small temperature

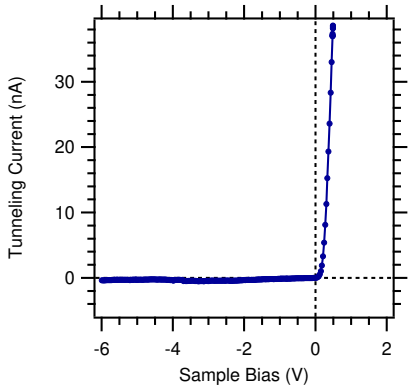

FIG. 5. Current versus voltage curve acquired by advanced lab students from the p-type Si sample. The data show rectifying behavior, suggesting a Schottky barrier.

fluctuations. Because we operate the ZTM without a feedback loop, there is the potential for significant change in tip-sample separation (and thus tunneling current) without user intervention. Attention to this possibility is essential. Each time the tip comes into range, we examine the tunneling current as a function of time for a few minutes before acquiring data. Figure 6 shows a representative plot of the tunneling current versus time acquired with a HOPG sample in place. Problematic changes of $\sim$ 0.1 nA over 20-30 seconds are marked with arrows (1 and 2). However, between locations 1 and 2, the current remains stable to within 0.1 nA for 200 seconds, an order of magnitude longer than the time it takes to acquire an I-z or I-V curve. To encourage these optimal conditions, we also take care in preparing the sample to be as flat as possible, and the enclosure with acoustic panels appears to minimize thermal drift. We also note that in scanning tunneling microscopy, the feedback loop is typically shut off prior to acquisition of I-z or I-V curves.

VI. CONCLUSION

In conclusion, we have built a simplified alternative to a STM that limits tip motion to the z-axis alone—the ZTM. This instrument can be customized to fit the needs of individual departments in several ways. Material costs for the ZTM are relatively inexpensive, and its required input and output voltages can be integrated with data acquisition tools or

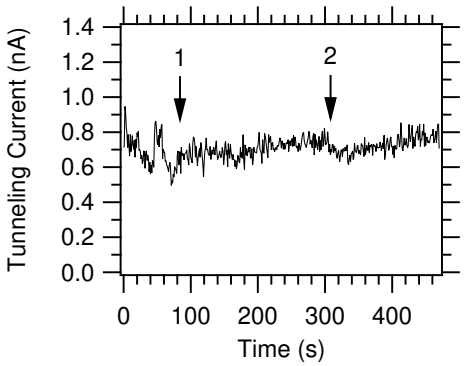

FIG. 6. Representative plot of tunneling current versus time (HOPG sample). Here, the average current is stable to within 0.1 nA for about 200 seconds (between locations 1 and 2 as marked). For comparison, typical I-z and I-V sweeps take $\lesssim 10$ seconds.

electronics that typically exist in an instructional laboratory. While our form factor for the body was two aluminum slabs, the ZTM concept could be implemented in other simple form factors that have been used to construct STMs.[1–4] Others may choose to operate the ZTM in a dry nitrogen box or glove bag, and we presume this could improve the accuracy of the measured work functions in the I-z data. In addition to tunneling measurements, the ZTM may be used as an ambient point-contact spectroscopy probe.

Regardless of specific customizations, the principle of the z-axis tunneling microscope is useful for producing lab equipment to study tunneling and basic electronic structure. Students using the ZTM gain experience in experimental methods of condensed matter physics, learning about electronic structure of materials, work functions, and tunneling probabilities. The ZTM has been used successfully in an advanced instructional lab setting, but it may also be appropriate for other levels of the undergraduate curriculum (e.g., modern physics instructional lab, independent senior projects).

ACKNOWLEDGMENTS

We gratefully acknowledge George McBane for helpful discussions and material support. This work was supported in part by the Center for Scholarly and Creative Excellence at

Grand Valley State University.

* veazeyj@gvsu.edu

[1] R. A. Lewis, S. A. Gower, and P. Groombridge, "Student scanning tunneling microscope," Am. J. Phys. **59**, 38 (1991).

[2] P. J. Williams, D. White, and K. Mossman, "A simple scanning tunneling microscope," Am. J. Phys. **65**, 160 (1997).

[3] T. Ekkens, "A student-built scanning tunneling microscope," Phys. Teach. **53**, 539–541 (2015).

[4] D. Berard, Home-built STM website, <https://dberard.com/home-built-stm/>.

[5] Y. G. Naidyuk and I. K. Yanson, *Point-contact spectroscopy* (Springer, New York, NY, 2005).

[6] G. Binnig, H. Rohrer, C. Gerber, and E. Weibel, "Tunneling through a controllable vacuum gap," Appl. Phys. Lett. **40**, 123711 (1982).

[7] S. I. Park and C. F. Quate, "Tunneling microscopy of graphite in air," Appl. Phys. Lett. **48**, 112–114 (1986).

[8] A. Tomic, Z. Rak, J. P. Veazey, S. D. Mahanti, S. H. Tessmer, C. D. Malliakas, and M. G. Kanatzidis, "Scanning tunneling microscopy study of the $CeTe_3$ charge density wave," Phys. Rev. B **79**, 7 (2008).

[9] J. Bardeen, "Tunnelling from a many-particle point of view," Phys. Rev. Lett. **6**, 57–59 (1961).

[10] B. Voigtländer, "Scanning tunneling microscopy," in *Scanning Probe Microscopy: Atomic Force Microscopy and Scanning Tunneling Microscopy* (Springer Berlin, Heidelberg, 2015), p. 279–308.

[11] J. A. Stroscio, R. M. Feenstra, and A. P. Fein, "Electronic Structure of the Si(111)2 × 1 surface by scanning-tunneling microscopy," Phys. Rev. Lett. *57*, 2579 (1986).

[12] X. Zhang, K. Wang, W. Chen, M. M. Loy, J. N. Wang, and X. Xiao, "Electrical transport through a scanning tunnelling microscope tip and a heavily doped Si contact," J. Appl. Phys. **114**, 013701 (2013).

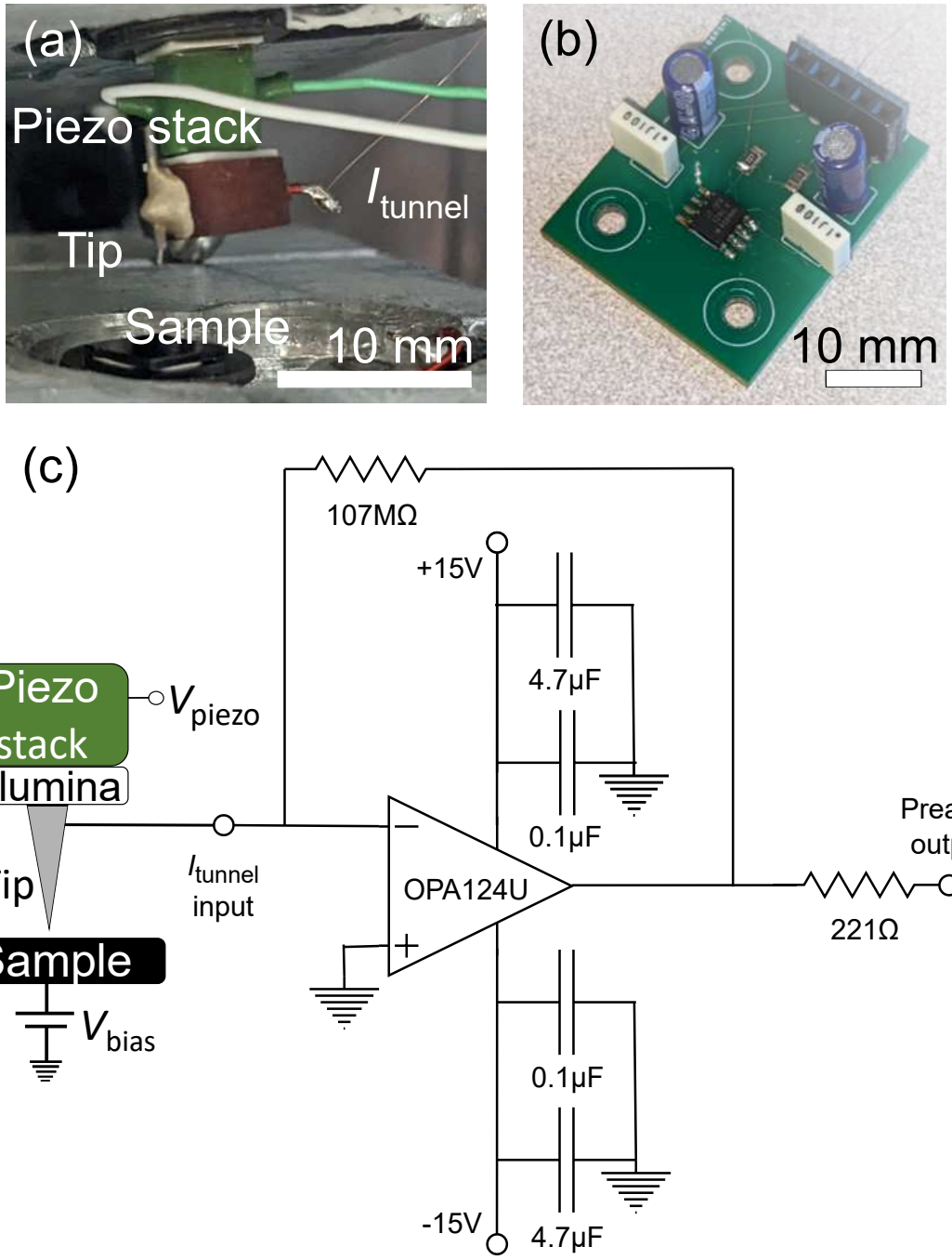

AMERICAN JOURNAL OF PHYSICS

PLEASE CITE THIS ARTICLE AS DOI: 10.1119/5.0094028

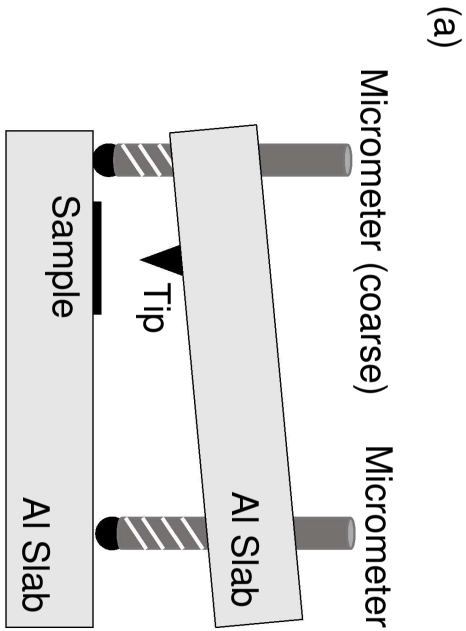

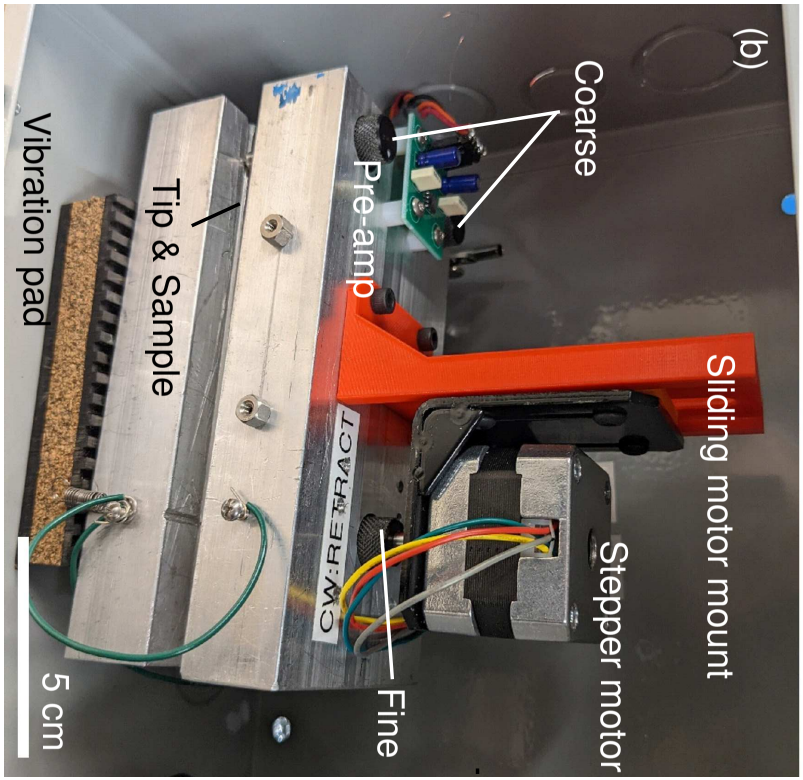

AAPT PHYSICS EDUCATION®
AMERICAN JOURNAL OF PHYSICS

PLEASE CITE THIS ARTICLE AS DOI: 10.1119/5.0094028

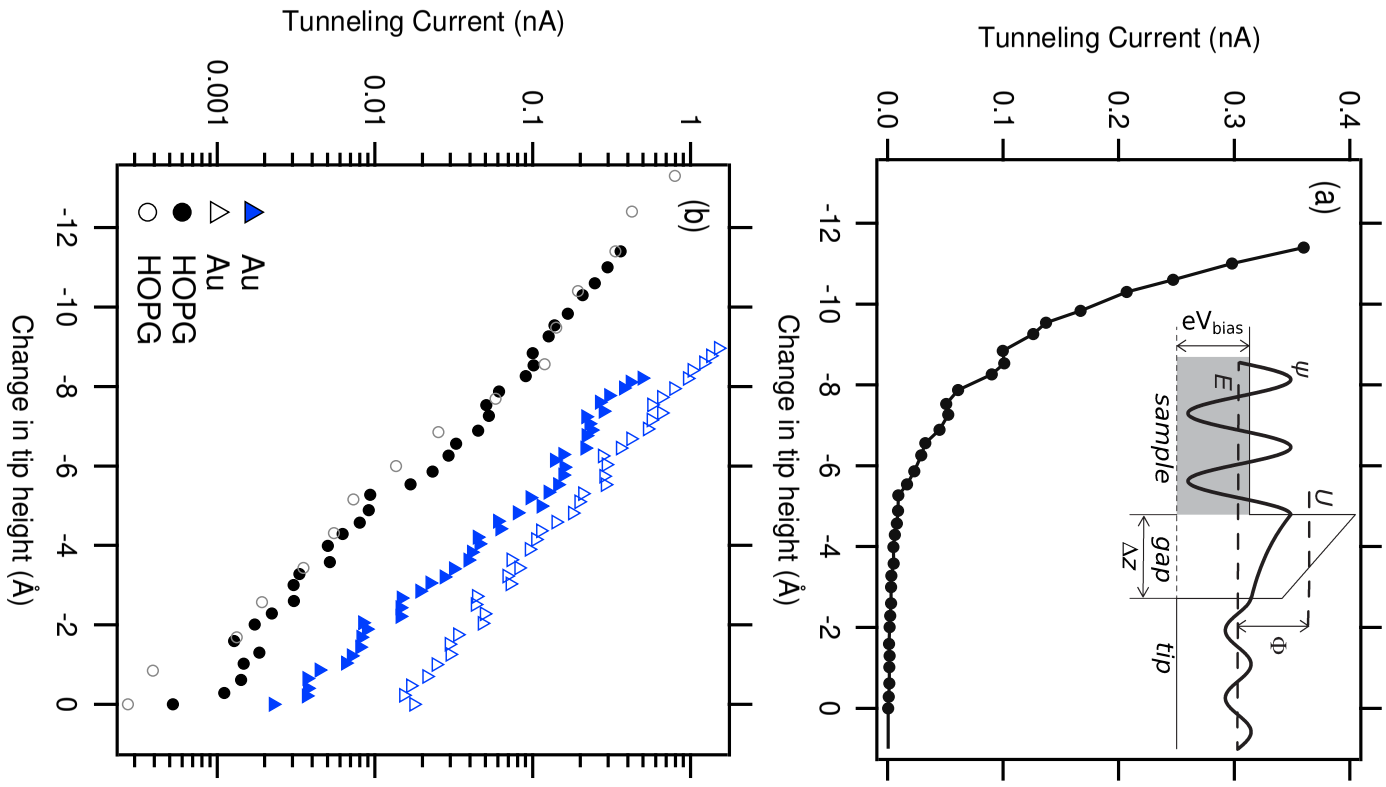

AAPT PHYSICS EDUCATION®
AMERICAN JOURNAL OF PHYSICS

PLEASE CITE THIS ARTICLE AS DOI: 10.1119/5.0094028

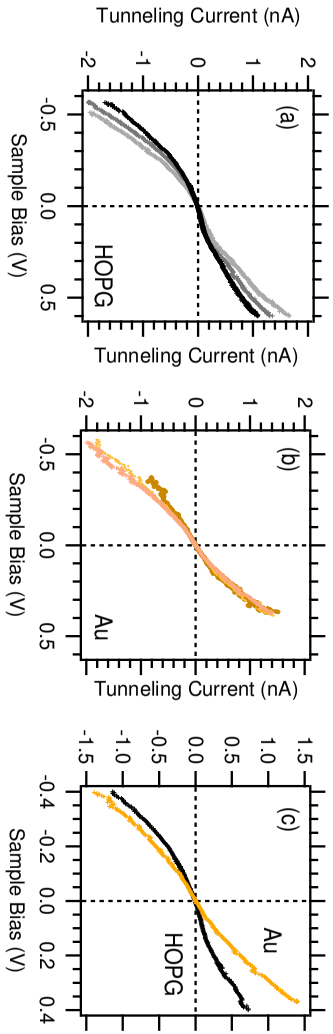

AAPT PHYSICS EDUCATION®
AMERICAN JOURNAL OF PHYSICS

PLEASE CITE THIS ARTICLE AS DOI: 10.1119/5.0094028

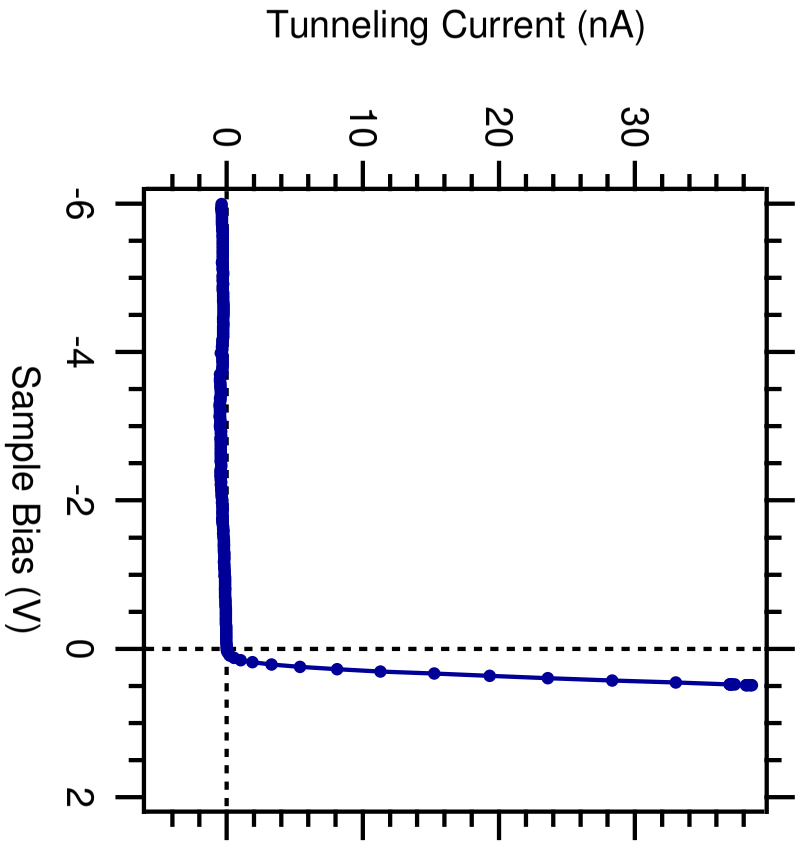

AAPT PHYSICS EDUCATION®
AMERICAN JOURNAL OF PHYSICS

PLEASE CITE THIS ARTICLE AS DOI: 10.1119/5.0094028